Geophys. J. Int. (2008) **172,** 1123–1134 doi: 10.1111/j.1365-246X.2007.03701.x

Seismo-acoustic analysis of the Buncefield oil depot explosion in the UK, 2005 December 11

L. Ottemöller[1] and L. G. Evers[2]

[1]*British Geological Survey (BGS), Murchison House, West Mains Road, Edinburgh* EH9 3LA*, UK. E-mail: lot@bgs.ac.uk*
[2]*Royal Netherlands Meteorological Institute (KNMI), Wilhelminalaan* 10, NL-3732 *GK, De Bilt, the Netherlands*

Accepted 2007 November 27. Received 2007 September 25; in original form 2007 February 6

SUMMARY

A massive vapour cloud explosion occurred at the Buncefield fuel depot near Hemel Hempstead, UK, in the morning of 2005 December 11. The explosion was the result of an overflow from one of the storage tanks with the release of over 300 tons of petrol and generating a vapour cloud that spread over an area of 80 000 m^2, before being ignited. Considerable damage was caused in the vicinity of the explosion and a total of 43 people were injured. The explosion was detected by seismograph stations in the UK and the Netherlands and by infrasound arrays in the Netherlands. We analysed the seismic recordings to determine the origin time of 06:01:31.45 $\pm$0.5 s (UTC) from *P*-wave arrival times. Uncertainties in determination of origin time from acoustic arrival times alone were less than 10 s. Amplitudes of *P*-, *Lg* and primary acoustic waves were measured to derive decay relationships as function of distance. From the seismic amplitudes we estimated a yield of 2–10 tons equivalent to a buried explosion. Most seismic stations recorded primary and secondary acoustic waves. We used atmospheric ray tracing to identify the various travel paths, which depend on temperature and wind speed as function of altitude, leading to directional variation. Refracted waves were observed from the troposphere, stratosphere and thermosphere with a good match between observed and calculated traveltimes. The various wave types were also identified through array processing, which provides backazimuth and slowness, of recordings from an infrasound array in the Netherlands. The amplitude of stratospheric refracted acoustic waves recorded by the array microbarometers was used to estimate a yield of 21.6 ($\pm$5) tons TNT equivalent. We have demonstrated through joint seismo-acoustic analysis of the explosion that both the seismic velocity model and the atmospheric model are sufficient to explain the observed traveltimes.

1 INTRODUCTION

A massive explosion occurred at the Buncefield fuel depot near Hemel Hempstead, UK, just after 06:00 UTC (all times given are UTC) on 2005 December 11. Both seismic and acoustic waves from the explosion were detected at more than 30 seismic stations in the UK, and at seismic and infrasound stations in the Netherlands. Further explosions reported to have occurred within half an hour of the main explosion (Powell 2006c) were not detected by the seismic stations and, therefore, must have been significantly smaller. This study deals with the main explosion only.

The main explosion was a vapour cloud explosion (VCE) resulting from the overflow of unleaded petrol from a storage tank. The details of the events leading to the explosions are given in reports by the Buncefield investigation team (Powell 2006a,b,c). The Buncefield fuel depot with more than 20 tanks is one of the UK's largest storage facilities and on 11 December a total of 35 000 m^3 were held on site (Powell 2006a). The overflow started at 05:20 and for 33 min was at a rate of 550 m^3 hr^{-1}. The rate then increased to 890 m^3 hr^{-1} for 7 min, resulting in a total overflow of over 300 tons at the time of the explosion (Powell 2006c). This led to the formation of a vapour cloud over an area of about 80 000 m^2 with a thickness of 1–7 m before the explosion.

The explosion is thought to be the largest in Europe since the Second World War. A total of 43 people were injured. The explosion was followed by a fire of the remaining fuel that lasted for more than 36 hr. The explosion occurred above ground releasing both acoustic and seismic waves, which were both widely felt. However, damage was restricted to the vicinity (<2 km) of the explosion site. A macroseismic survey was carried out by the British Geological Survey (BGS) revealing that the explosion caused damage corresponding to 6 European Macroseismic Scale (EMS) over an area of 230 km^2 and was observed at intensity 2–3 EMS over an area of 130 000 km^2 (Roger Musson, personal communication, 2006).

The destructive potential of VCEs is well known (e.g. Tang & Baker 1999) and was experienced in the UK at a chemical plant

at Flixborough in 1974, when 28 workers were killed (Health and Safety Executive 1975). A smaller VCE after release of about 20 tons of hydrocarbons occurred in Milford Haven, UK, in 1994 (Health and Safety Executive 1997). Maremonti *et al.* (1999) analysed seismic data from a VCE that occurred near Naples (Italy) in 1985. They derived energy, the TNT equivalent and vapour volume from seismic recordings, which matched results from vapour cloud modelling. Another VCE occurred in Skikda, Algeria, in 2004 at a liquid natural gas production plant (http://www.energy.ca.gov, accessed 2006 April 19). The explosion of a gas pipeline in Ghislenghien, Belgium, was studied by combining seismic and infrasound data (Evers *et al.* 2007). Other examples of explosion sources studied using seismic data are the chemical plant explosion in Nevada (Ichinose *et al.* 1999) and the pipeline explosion in New Mexico (Koper *et al.* 2003).

This paper presents the combined analysis of seismic and acoustic wave observations. We use seismic wave arrival times to determine the explosion's origin time for the known location. We describe phase identification of acoustic waves observed on both seismic and infrasound instruments using atmospheric ray tracing and use these to validate the atmospheric model and origin time. We also investigate seismic amplitudes as a function of distance and derive the energy and yield of the explosion.

2 OBSERVATIONS

Both seismic and acoustic waves from the explosion were detected on seismic stations in the UK and the Netherlands (Figs 1 and 2). The acoustic waves were also observed at infrasound stations in the Netherlands (Fig. 1). The seismograms showed either a primary, a secondary or both acoustic arrivals. With primary we refer to the stratospheric refractions and call all later arrivals secondary. Most of the seismic stations in the UK are operated by the BGS. In addition, we used data from station WOL, which is operated by the Atomic Weapons Establishment (AWE) Blacknest. The seismic and infrasound stations in the Netherlands are operated by the Royal Netherlands Meteorological Institute (KNMI).

The recording at the closest seismic station from the explosion site (SKP, 27 km) was saturated and the data could only be used to determine the *P*-wave arrival time. Most stations used in this study are equipped with short-period seismometers and a few with broadband seismometers. However, as the signals from this explosion carry little energy below 0.5 Hz, there is no need to differentiate for the purpose of this study.

The acoustic waves were also recorded on two hydrophones installed at SWN (99 km) and HTL (295 km). Fig. 3 shows the comparison of pressure recorded on the hydrophone and ground velocity recorded on a vertical component seismometer, both at SWN (the acoustic wave at HTL was recorded only on the hydrophone). Both records (Fig. 3) show a high frequency signal of small amplitude that is followed by a larger amplitude, relatively low frequency, signal, which can be modelled by the presence of temperature inversion and wind shear (Green *et al.* 2006). The pressure and velocity signals are remarkably similar, as expected where the seismic records are caused by the pressure wave at the site (piston effect, e.g. Starovoit & Martysevich 2005). Comparison with earthquake recordings in the UK shows that the hydrophone at this distance and frequency range (0.5–5 Hz) is not affected by the seismic waves.

Almost no natural or man-made seismicity has been recorded from the area surrounding the Buncefield explosion site. Comparison with earthquakes from the wider region shows that recordings of *P* waves in terms of waveform complexity are generally not very different from those of the explosion. However, on average the *S*-wave amplitudes from earthquakes are larger than the respective *P*-wave amplitudes. Synthetic seismograms (Wang & Herrmann 1980; Herrmann & Wang 1985) were computed in the distance range 70–150 km using either an explosion source in air or a vertical force applied to the surface. Both sources practically gave the same results. The synthetic seismograms showed the same degree of complexity for *P* waves as the observed seismograms, but a meaningful comparison at these distances for frequencies in the range 2–5 Hz was not possible. The main outcome from the modelling was that a single explosion source is sufficient to explain the seismograms. However, the synthetic seismograms predict the observation of Rayleigh waves, which were not seen in the observed seismograms, probably due to high attenuation in the near-surface layers. Our nearest recording of the acoustic wave was at a distance of 27 km, which is too large to draw conclusions on the source duration or rise time of the pressure wave, as the acoustic waves are already significantly dispersed.

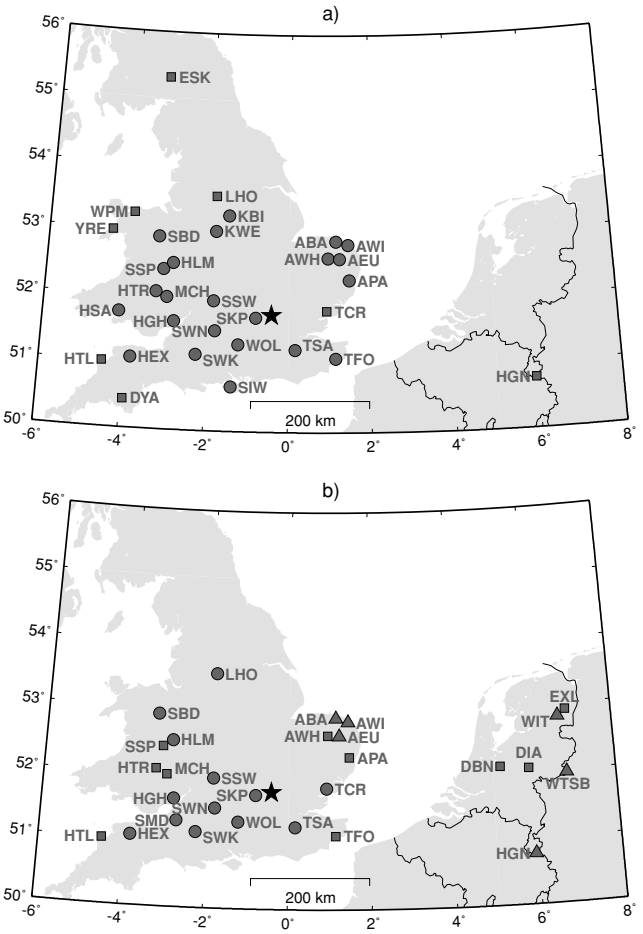

Figure 1. Overview of station locations and observations: (a) seismic stations that detected the seismic waves. Stations used to determine the origin time are indicated by a circle, stations that were not used are indicated by a square. (b) Seismic stations and infrasound array (DIA) that detected the acoustic waves. Circles give stations that detected only the primary wave, triangles gives stations that detected only refracted waves, and squares detected both types of acoustic waves.

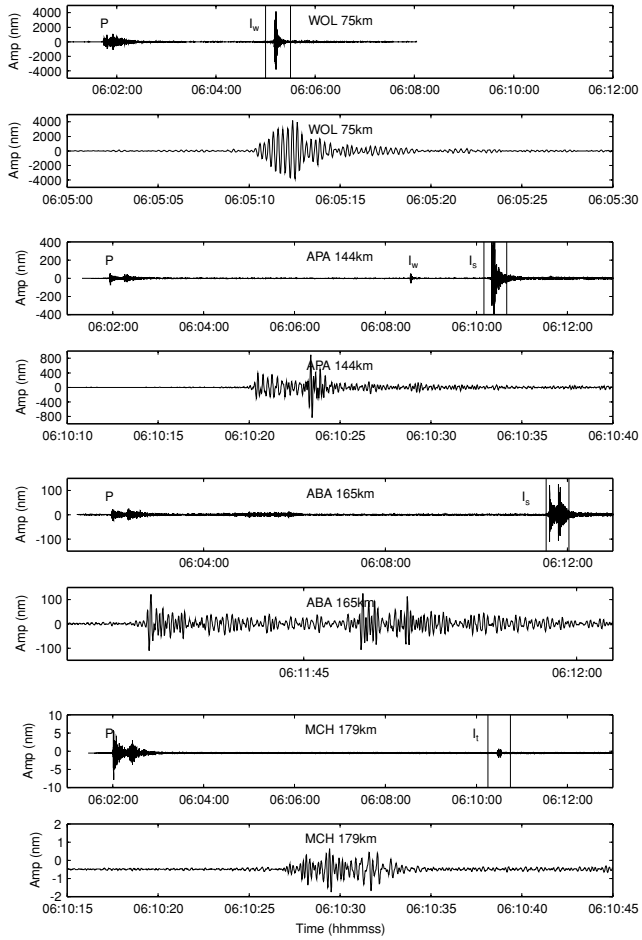

Figure 2. Displacement seismograms bandpass filtered 3–8 Hz for four stations. The top traces for each station display 12 min of data showing both seismic and infrasound waves. Seismic *P* waves are indicated by *P*, and infrasound waves Iw, Is and It (see section on infrasound propagation for details). The bottom traces for each station show: tropospheric arrivals for stations WOL, APA and MCH, and arrivals from greater altitude for stations APA and ABA. The time windows are marked on the respective top traces. Both tropospheric arrival and higher altitude arrival are seen on station APA, the latter has a significantly larger amplitude.

3 SEISMIC WAVE INTERPRETATION AND RESULTS

3.1 Origin time

The location of the explosion at the Buncefield fuel depot site is approximately (±150 m) 51.766°N latitude and 0.427°W longitude. The explosion occurred on the surface. As the location of the explosion is known, seismic wave arrival times can be inverted for the origin time only. A total of 21 seismic *P*-wave arrivals were used from seismic stations in the UK at distances of 27–247 km (Fig. 1). The accuracy of phase arrivals determined by manual 'picking' is approximately 0.1 s. Having sufficient *P*-wave arrivals, we did not use *S*-wave arrivals as their picking is slightly less accurate. The origin time was computed using the HYPOCENTER location program (Lienert 1994; Lienert & Havskov 1995). No station- or distance-dependent weighting of the arrival times was applied. Formal errors were computed for a 90 per cent confidence interval.

Several regional 1-D velocity models are in use at the BGS for locating earthquakes in the UK (Booth *et al.* 2001). However, no specific model has been derived for central England, including the region around the explosion site. The model derived for Mid Wales (Edwards & Blundell 1984) (Table 1) is the one in use at the closest distance to the Buncefield explosion and, therefore, expected to provide the most valid approximation. The origin time computed for the Mid Wales model is 06:01:31.45 UTC (±0.5 s). The corresponding traveltimes are shown in Fig. 4. Results based on an average UK model (Assumpção & Bamford 1978; Bamford *et al.* 1978) were slightly worse (Ottemöller 2006) and are not given here.

We also solved the inverse problem by locating for both location and origin time for a fixed depth of 0 km to verify the location procedure and velocity model and to determine a robust uncertainty of the origin time. The location obtained through inversion using the Mid Wales model is shifted from the actual location by 1.4 km to the northwest, the origin time is increased by 0.1 s and the rms remains practically unchanged. The computed horizontal error in epicentre location is 1.5 km, which only just includes the actual explosion site. The change in origin time is well within the formal error of 0.5 s. The difference between true and computed location of only 1.4 km shows that the Mid Wales model is appropriate for this analysis.

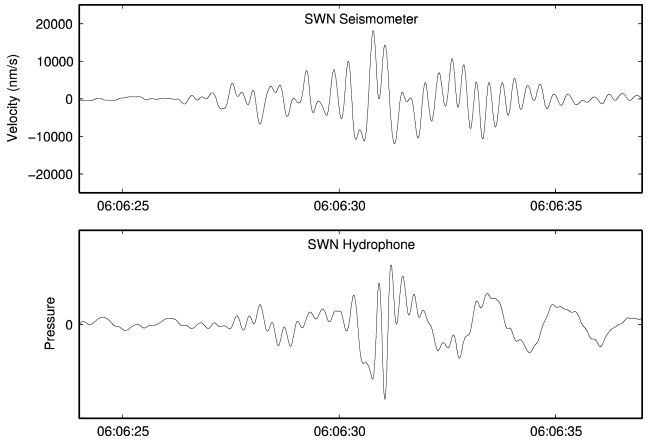

Figure 3. Comparison of vertical component seismometer (velocity) and hydrophone recordings of the primary acoustic wave at SWN at a distance of 99 km from the source. The data is bandpass filtered 0.5–5 Hz. Units of pressure are not given as the pressure sensor is installed inside a building and not calibrated.

Table 1. Mid Wales velocity model.

Depth to top of layer (km)	*P*-wave velocity (km s^{-1})
0.0	5.40
3.8	6.05
15.5	6.65
34.3	8.00

3.2 Amplitudes

Displacement amplitudes were measured on 1–20 Hz bandpass filtered seismograms for *P*, *Lg* (multiply-reflected *S* waves trapped in the crust) and the primary acoustic waves (Fig. 5). The acoustic wave amplitudes are the largest at distances of less than 162 km, but decay faster with distance than *P*- and *Lg*-wave amplitudes. Beyond 162 km, *P*-wave amplitudes are generally largest. For some stations, the refracted acoustic waves have the largest amplitude (Fig. 2). Most people who felt the explosion were within about 50 km of the

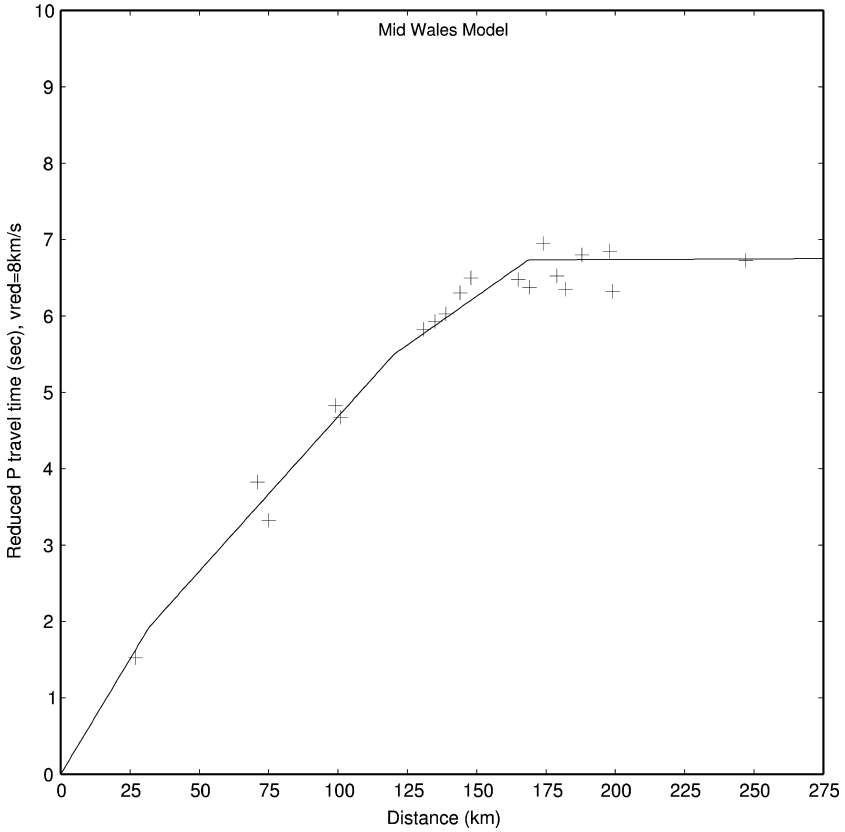

Figure 4. Reduced traveltime plot for first arriving *P* wave showing observations (plus symbols) and traveltimes calculated for the Mid Wales velocity model (solid line).

explosion site. Reports indicated that people felt the arrival of both seismic and acoustic waves. Although there is a lack of measurements at distances less than 70 km, it is likely that the acoustic waves were felt more strongly.

The amplitude ratios between *P* and acoustic waves confirm the faster decay of acoustic wave amplitudes, seen as an increase of the ratio with distance (Fig. 5). The range of values for the ratio of *P* to acoustic wave amplitude is 0.1–6.8. The ratio of *P*- to *Lg*-wave amplitude values was in the range 0.6–6.5, but as expected for an explosion source, most values are above 1. Variation of the amplitude ratio with azimuth is not significant (Fig. 5), which means that deriving relations for amplitude decay as a function of distance only is justified. The results from least-squares linear regression are given in Table 2 and plotted with the observed data in Fig. 5. The decay of amplitudes with distance of *P* waves is slightly faster than that of *Lg*-wave amplitudes. The coefficient *a* determined from *Lg* waves here is very similar to the result obtained when inverting average *Lg*-wave amplitudes for the UK (Table 2).

3.3 Energy and yield

While source scaling of chemical explosions has been studied, this to our knowledge has not been done for VCEs. We therefore, measure seismic amplitudes and derive the yield of a buried chemical explosion equivalent to the size of the Buncefield explosion through comparison with other explosion types.

A local magnitude of 2.2 ML was computed as average from the largest amplitudes measured from *P* wave Wood-Anderson simulated records at 22 stations (70–295 km). The ML formula (Hutton & Boore 1987) used in the UK is

$$\mathrm{ML} = \log(A) + 1.11\log(D) + 0.00189 \times D - 2.09, \quad (1)$$

where the amplitude (A) is in nm and the distance (D) in km. *P*-wave amplitudes were used as they are the largest, although standard practice for earthquakes is to use *S*-wave amplitudes.

Khalturin *et al.* (1998) showed that there is no simple relationship between the yield of chemical explosions and magnitude, and that the magnitude deficit can be as large as 2 mag units. For a set of explosions with known yield, they derive a relationship for the upper limit of magnitude with yield. Comparison with their data set shows that a magnitude of 2.2 ML, as measured for the Buncefield explosion, could be observed for yields between 3 and 250 tons. Comparison with quarry blasts in the UK (Jacob & Neilson 1977) shows that values around 2.2 ML have been observed for quarry blasts with charge sizes of 2–10 tons. The large spread, when comparing yield and magnitude for chemical explosions, is caused by the strong variation in coupling. We expect that the spread is even larger for VCEs due to large coupling uncertainties. The magnitude of earthquakes can also be converted to energy (Stein & Wysession 2003)

$$\log E = 1.5M_{\mathrm{w}} + 4.8. \quad (2)$$

For a magnitude of 2.2, this gives 126 MJ radiated seismic energy. This energy can be converted to the yield of an explosion that is required to release the same amount of seismic energy (Evernden *et al.* 1986; Lahr 1999) where 63.1 MJ is equivalent to 1 ton TNT. This conversion is based on the observation that a 1 kton explosion is approximately equivalent to a magnitude 4 earthquake. Applying

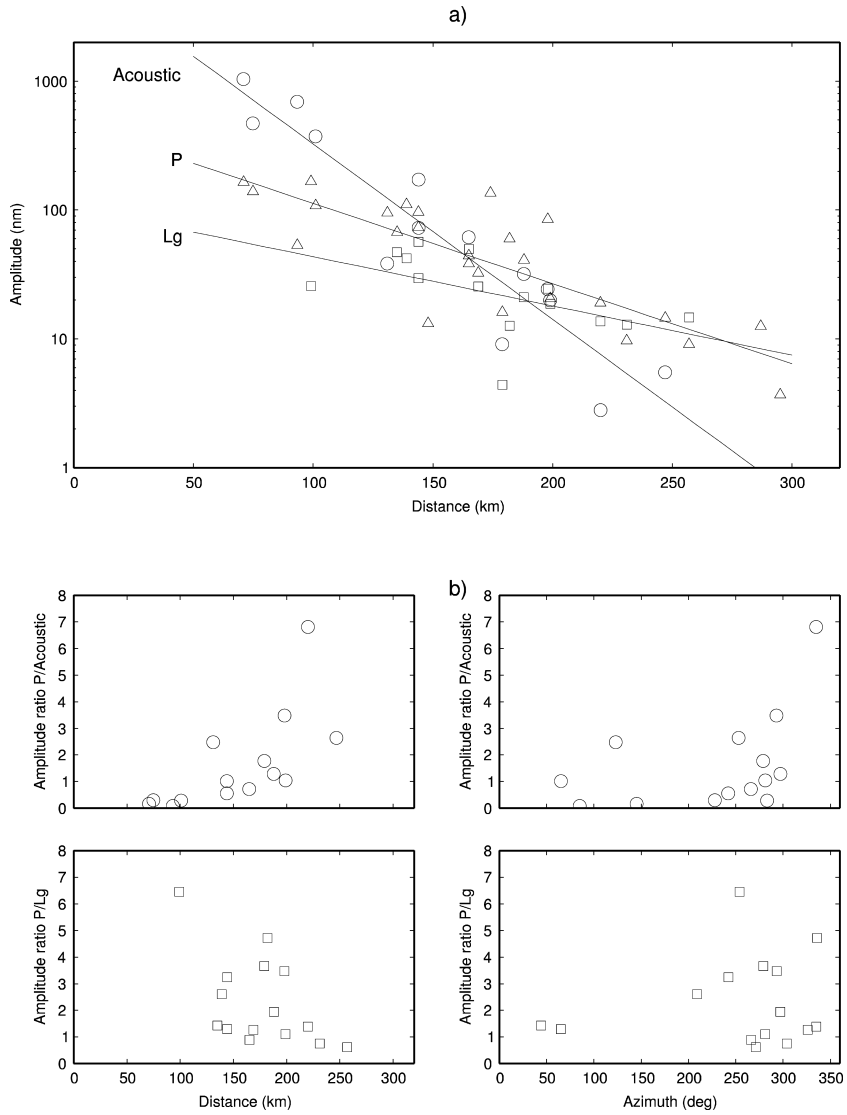

Figure 5. (a) Maximum displacement amplitudes in the frequency band 1–20 Hz of seismic *P* (triangles) and *Lg* waves (squares) and amplitudes of primary acoustic waves observed (circles) on the seismic stations as a function of distance. For comparison, the solid lines give the amplitudes based on the regression results (Table 2) for primary acoustic, *P*- and *Lg*-wave, respectively. (b) Ratios of *P*/Acoustic and *P*/*Lg* wave amplitudes as a function of distance (left-hand panels) and azimuth (right-hand panels).

Table 2. Least-squares regression for coefficients in $\log(A) = a \times D + b$; A is the amplitude in nm and D the distance in km; *SE* gives the standard error for a and b. For comparison we give an average a determined from maximum *Lg*-wave amplitudes observed on vertical component instruments in the UK.

Wave type	a	$SE(a)$	b	$SE(b)$
P	−0.00622	0.0009	2.67	0.15
Lg	−0.00382	0.0016	2.02	0.30
Direct acoustic	−0.01360	0.0015	3.87	0.24
Lg UK average	−0.00432	0.0002		

this, the seismic energy released by the Buncefield explosion is equivalent to 2 tons TNT.

Experiments carried out near nuclear test sites show that the yield for a defined earthquake magnitude also depends on the attenuative properties of the local geology. For the US Nevada test site (NTS), where seismic wave attenuation is high, Murphy (1981) determined that

$$m_b = 3.92 + 0.71 \log Y, \tag{3}$$

where mb is the body wave magnitude and Y is yield in kilotons of TNT. For low attenuation regions such as the former Kazakh test site, Ringdal *et al.* (1992) found that

$$m_b = 4.45 + 0.75 \log Y. \tag{4}$$

For magnitude ML 2.2 (assuming ML = mb), the corresponding yields range from 1 ton TNT to 7.5 tons TNT.

Evans (1999) determined a relationship for charge size scaled velocity amplitude (SVEL) with distance. The relationship is valid for quarry blasts in the UK and distances of up to 100 km. Velocity amplitudes measured at three stations (TSA 71 km, SWN 99 km and SSW 101 km) give a charge size in the range of 2.5–25 tons TNT for the Buncefield explosion.

4 INFRASOUND PROPAGATION THROUGH THE ATMOSPHERE

The atmosphere is a highly anisotropic medium where propagation of infrasound is controlled by the sound speed. The amplitude and direction of the wind field changes with altitude making the sound speed azimuth dependent. Furthermore, the sound speed is influenced by strong temperature gradients in distinct regions within the atmosphere. The effective sound speed (v_{eff}) is the combination of the sound speed dependent on the absolute temperature (T) and the projection of the wind ($\vec{u}$) onto the path from source to receiver ($\hat{n} \cdot \vec{u}$)

$$v_{\text{eff}} = \sqrt{\gamma_g r T} + \hat{n} \cdot \vec{u}. \quad (5)$$

The product of the specific heat ratio (γ_g) with gas constant (r) for air is $\gamma_g r = 402.8\,\text{m}^2\,(\text{s}^2\,\text{K})^{-1}$, (e.g. Gossard & Hooke 1975). The atmosphere is divided into several layers based on the temperature gradient. Each layer is confined by a change of slope of temperature as a function of altitude. Areas of constant temperature are called the tropopause, stratopause and mesopause (e.g. Andrews *et al.* 1987) (Fig. 6). We used two atmospheric models: the ECMWF model developed by the European Centre for Medium-Range Weather Forecasts; and the ground-to-space (G2S) model of the United States Naval Research Laboratory (NRL) (Drob *et al.* 2003). The latter can combine ECMWF and the climatological Horizontal Wind Model/Mass Spectrometer and Incoherent Scatter Radar Extended Model (HWM/MSISE) (Hedin *et al.* 1996). In this case, data from NASA's GOES4 was spectrally combined with HWM/MSISE into the G2S model. The two right-hand frames in Fig. 6 show the two components of the wind field, being the zonal and meridional wind. A positive value for the zonal wind implies a west to east direction. The meridional wind has a positive sign when directed from south to north. The HWM/MSISE model is supported by measurements from satellites and rocketsondes, giving a more reliable statistical description of the upper atmosphere than the ECMWF model. Therefore, preference should be given to the G2S model in the region where both models diverge around 40 km altitude.

Infrasound can be refracted from regions in the atmosphere where v_{eff} becomes larger than the value at the surface. The three most important areas are (1) the troposphere, in the case of a temperature inversion due to an increase in temperature with altitude; this may extend from the surface up to hundreds of metres or several kilometres altitude. (2) A combined wind and temperature effect in the upper stratosphere where both the polar vortex and absorption of solar radiation by ozone can contribute to high values of v_{eff}. Observation of stratospheric arrivals depends on the sign of the stratospheric zonal winds with respect to the source–receiver azimuth. During the Northern hemisphere winter, the polar vortex is directed from west to east, while in summer its direction changes by 180°, controlled by the temperature difference between the equatorial and polar atmosphere. (3) The lack of absorption of solar radiation in the thermosphere leads to high temperatures and consequently refraction of infrasound. Thermospheric refractions are always predicted, but observation depends on the source–receiver distance due to the high attenuation within this atmospheric layer (Bass & Sutherland 2004).

4.1 Phase identification with tau-p ray tracing and comparison with observations at seismic stations

Ray tracing through atmospheric models enables the identification of received phases. The tau-p method as used in seismology (Buland & Chapman 1983) was rewritten for the atmosphere, treating it as a moving medium, by Garcés *et al.* (1998). Ray trajectories of infrasound through NRL-G2S models are shown in Fig. 7.

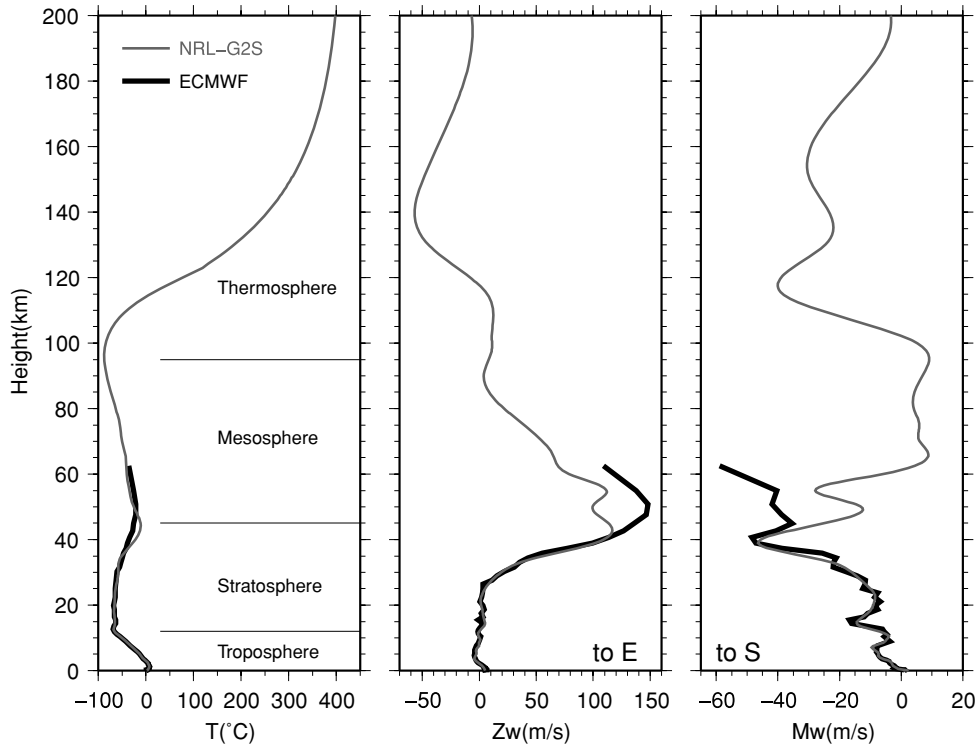

Figure 6. Atmospheric temperature and wind models from ECMWF and the NRL-G2S model. These models are valid for 52° latitude and 359.5° longitude on 2005 December 11 06h00 UTC.

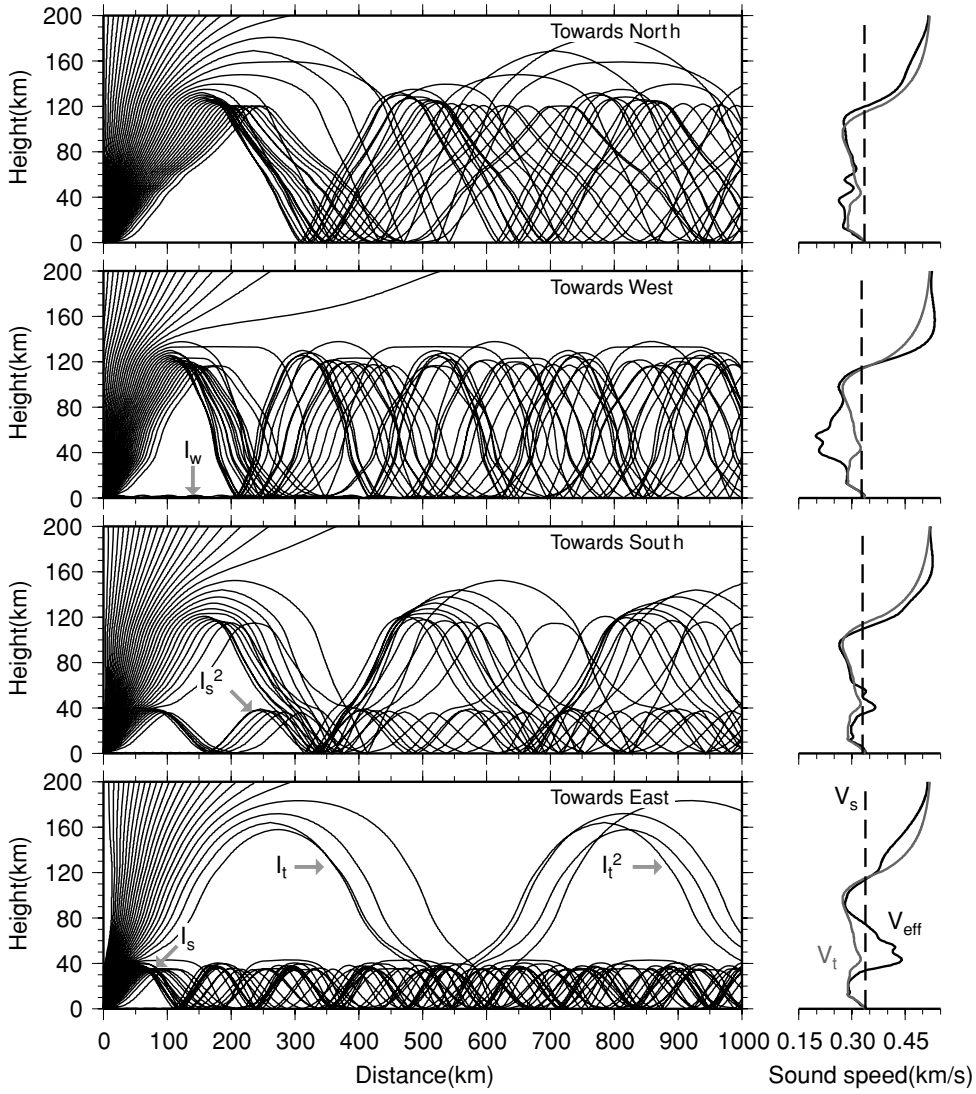

Figure 7. Ray trajectories of infrasound travelling from Buncefield towards the east (lower), south, west and north (upper frame). The velocity models, to right-hand side of the frames, give the effective sound speed at the surface (v_s) as vertical dashed line, the temperature dependent sound speed (v_t) in grey, and effective sound speed (v_{eff}) in black. These models are derived from the NRL-G2S model in Fig. 6.

Arrivals from the regions where v_{eff} becomes larger than its surface value are denoted I_w for tropospheric, I_s for stratospheric and I_t for thermospheric arrivals (Brown *et al.* 2002). In this paper, a superscript is added in case of multiple refractions between the Earth's surface and a refractive layer, so-called 'hops'. For example, a stratospheric phase that has made three hops on its way from source to receiver is identified as I_s^3.

The left-hand frames of Fig. 8 give the bounce points on the earth's surface, where from top to bottom: I_w, I_s and I_t are considered. The coloured dots give the type of acoustic observations at the seismic stations. I_w phases are trapped in an inversion layer with its top at 1 km altitude. These phases are present in most directions except roughly north to east because of the southward signature of the meridional wind. I_s arrivals are present to the east of Buncefield because of the eastward directed zonal stratospheric wind, that is, the polar vortex. I_s is present between 100 and 160 km distance while I_s^2 occurs from 200 km and starts interfering with I_s^3 from 300 km, somewhat further away, around 400 km, I_s^4 starts arriving. Beyond a shadow zone of 200 km to the west and 500 km east, I_t arrivals are modelled. The exceptionally small shadow zone of 200 km is caused by the strong counteracting stratospheric winds. Even I_t^2 is present to the west because of its small shadow.

Additional information for phase identification comes from the observed traveltimes. These are plotted as coloured dots in the right-hand frames of Fig. 8 together with the modelled traveltimes given as contours. Traveltimes from stations having the primary arrival (grey and yellow dots on the left-hand side) are shown in the top right-hand frame. The modelled traveltimes for I_w phases match the observed ones with an average residual of 9.2 s. The limited thickness of the inversion layers makes it hard to distinguish between a direct and multiple refracted I_w phase since the effective horizontal velocity of the two phases is almost equal. To the east (middle frame) I_s is very well covered by the model. The average residual for the I_s phases is 3.8 s.

The three Dutch seismic stations have probably recorded both stratospheric, I_s^3 and I_s^4, and thermospheric phases of type I_t. Due to this interference, modelled traveltimes do not match the observed ones. Later arrivals at stations to the west of Buncefield are of

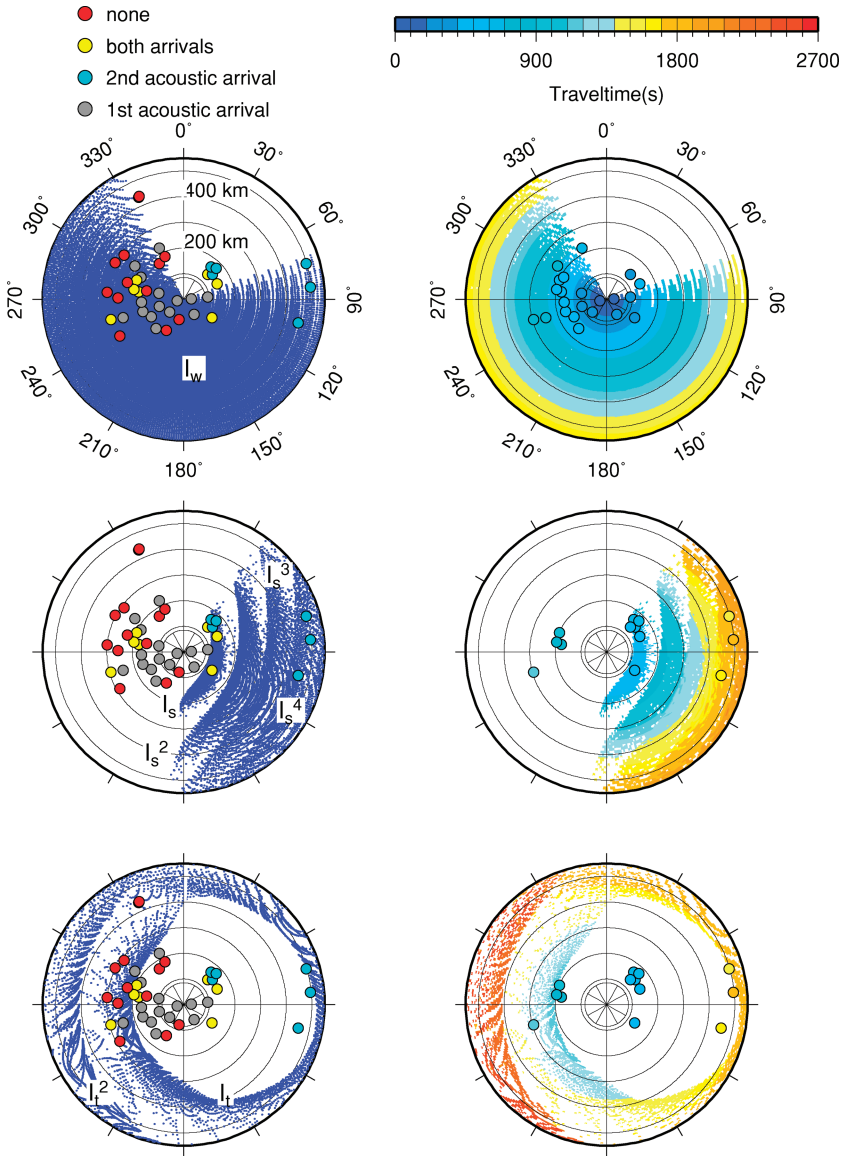

Figure 8. Ray tracing results from Buncefield to the seismic stations in the UK and the Netherlands. The left-hand frames give the bounce points on the earth's surface for, from top to bottom, I_w, I_s and I_t. The coloured dots show the type of acoustic arrival at each station. A station can either observe one primary acoustic arrival, grey dots, a secondary arrival, blue, the primary and one or more secondary arrivals, yellow, or no acoustic energy, red. The right-hand frames give the modelled traveltimess as contours and the observed times in coloured dots.

thermospheric origin. The predicted shadow zone is larger than observed, resulting in unreliably modelled traveltimes.

The origin time was computed by subtracting the modelled traveltimes from the arrival times and taking the mean of the values determined from the various stations. The origin time was determined as 06:01:23.2 (±6.6) and 06:01:26.5 (±2.6) from 20 tropospheric and 6 stratospheric arrivals, respectively.

4.2 Processing of infrasound array data

Energy from the explosion was recorded on three infrasound arrays in the Netherlands, see Fig. 1. The dominant frequency of the infrasonic signals over the Netherlands was 0.4 Hz. We concentrate on the data from the largest array, that is, the Deelen Infrasound Array (DIA). DIA consists of 16 microbarometers in an array of 1.5 km aperture. At the time of the explosion 10 microbarometers were operational. The other arrays (DBN and EXL) are much smaller, having apertures of 70–200 m and equipped with 6 microbarometers. Therefore, these arrays are less well suited to perform array processing of this low frequent event, although clear signals were observed.

The detection of events from infrasound array data is based on signal coherency. We use the Fisher ratio (S_F) as the measure of coherency (Melton & Bailey 1957). A detection is made when a measure of signal coherency becomes larger than some threshold value. In doing so, statistical relevance can be given to each detection. Furthermore, the number of false alarms and missed events can be mapped. The S_F is a scaled measure of signal-to-noise power ratio (*snr*) and describes the signal likelihood. The *snr* can be calculated from the S_F, assuming uncorrelated noise and plane waves, using

$$S_F = 1 + N \cdot snr. \quad (6)$$

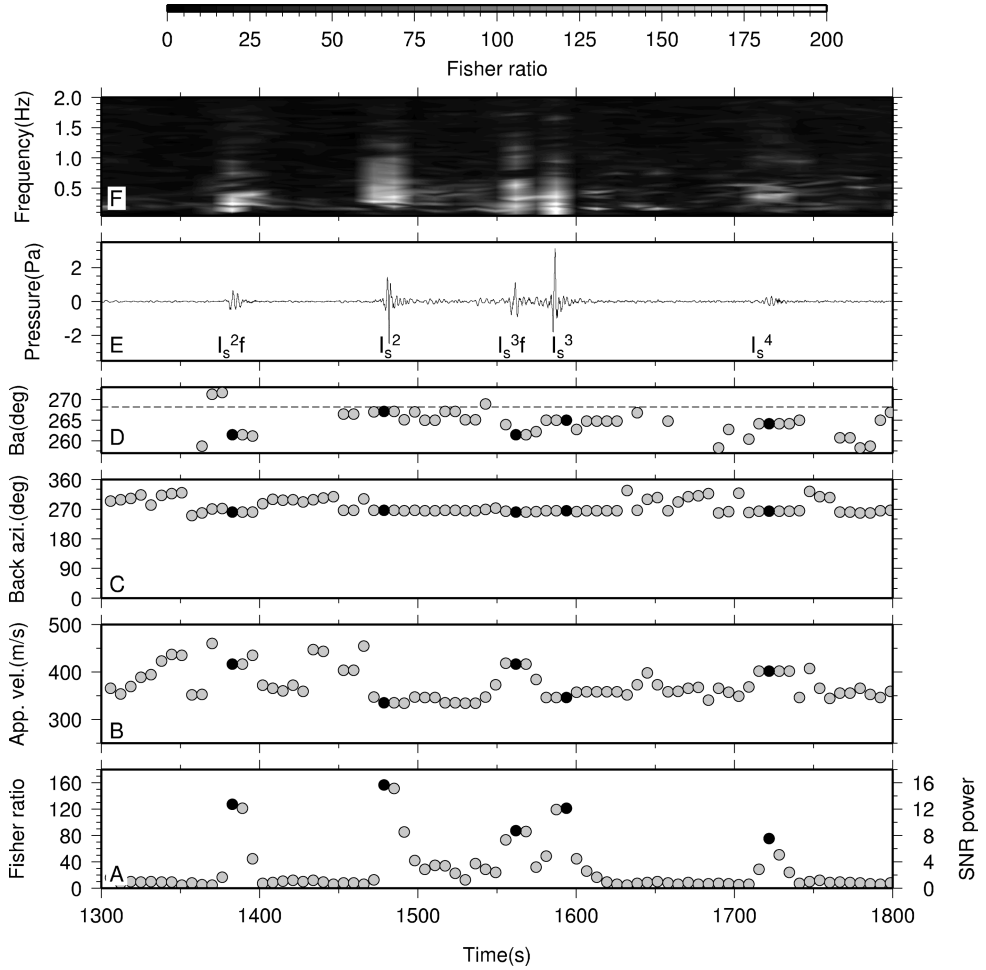

Figure 9. Results of the analysis of DIA data, bandpass filtered between 0.05 and 5 Hz. The horizontal axis is the time in seconds after the explosion occurred at 06h01m31.45s. The lowest frame (a) shows the maximum time domain Fisher ratios, or signal-to-noise power ratios, in 12.8 s time windows (512 samples at 40 Hz sample rate) with 50 per cent overlap. The resolved apparent velocity (b) and backazimuth (c) are evaluated on a 100 × 100 slowness grid. The small frame (d) enhances the deviations from the true backazimuth (dashed line). The best beam (e) is calculated for the most coherent event around 1480 s. The various infrasonic phases are also labelled, both regular and forerunner (*f*) arrivals are identified. Frequency domain results are given in the top frame (f) for 25.6 s and 50 per cent overlapping time windows.

The lowest frame (A) of Fig. 9 shows S_F as function of time since the explosion's origin time. Around the expected time of arrival of the energy over DIA, several strong increases in S_F are notable up to roughly a *snr* of 16. S_F is evaluated by beamforming in the slowness domain $\vec{p}$ which is the reciprocal of the apparent sound speed. At maximum S_F event characteristics in terms of apparent sound speed ($\vec{c}$) and backazimuth (ϕ) are resolved for that specific beam. The resolved apparent sound speeds $\vec{c}$ show an alternating sequence of high and low apparent sound speeds (Fig. 9b). The high values imply a steep angle of incidence of the energy typical for infrasound turning at large altitudes in the atmosphere. The backazimuths (Figs 9c and d) all point roughly in the direction of Buncefield and need to be corrected for the deviating effects of cross winds. The best beam in Fig. 9(e) is the sum of the phase-aligned traces in the direction of the most coherent event around 1480 s. In general, there appears to be a trend of phases with either high $\vec{c}$, large ϕ deviations and low amplitudes or low $\vec{c}$, small ϕ deviations and large amplitudes. This indicates propagation over different paths through the atmosphere, leading to different refraction altitudes and path lengths, other damping parameters and experience of cross winds. The higher and/or longer the energy travels into the stratosphere the more damping it will experience, leading to lower amplitudes. The orientation of the wave front will also be more deviated since cross winds can longer affect the original bearing. Large refraction altitudes are furthermore supported by the high apparent velocities. In summary, the alternating sequence of phases corresponds to low (35 km) and high (45 km) stratospheric refractions. Evers & Haak (2007) identified these arrivals as exceptionally fast acoustic phases or forerunners. The forerunners have been trapped in a high velocity acoustic channel at around 40 km altitude. These head-wave like propagation paths explains their early arrival, high $\vec{c}$ and large ϕ. The various phases are labelled in frame e of Fig. 9.

The Fisher ratio is also described in the frequency domain by Smart & Flinn (1971). Fig. 9(f) shows the results of the Fisher statistics in the frequency domain. The frequency content of the signals is in the interval 0.06 and 1.8 Hz, being dominant around 0.4 Hz. The high frequency contents of the upper stratospheric refractions appears to be lost due to damping. However, care should be taken with this interpretation since more impulse-like signals, that is, the low stratospheric phases, intrinsically have a broader frequency spectrum.

4.3 Yield estimation from infrasound records

The yield of the explosion is estimated from infrasound records by comparing the observed amplitudes with the high explosives (HE) data set from Los Alamos National Laboratory (Davidson & Whitaker 1992; Evers *et al.* 2007). The data set consists of 27 shots of mainly Ammonium Nitrate Fuel Oil (ANFO), a widely used explosive. The high explosive shots cover a range of charge weights from 20 to 4880 tons and were observed with infrasound instrumentation over distances between 250 and 5330 km. The distance or range (R) in km is scaled with the charge weight (Y) in kilotons of high explosives to give the scaled range ($R_{\rm scaled}$)

$$R_{\rm scaled} = \frac{R}{\sqrt{2 \times Y}}. \quad (7)$$

Observed infrasonic phases are of I_s type and their raw amplitudes ($P_{\rm raw}$, peak-to-peak in mbars) are empirically corrected for the strongest stratospheric winds between 40 and 60 km altitude. The wind is projected in the direction from source to observing station using $\hat{n} \cdot \vec{u}$, as was done for calculating the effective sound speed in eq. (5). This wind contribution is then used to derive the wind-corrected amplitude $P_{\rm wca}$

$$\log(P_{\rm wca}) = \log(P_{\rm raw}) - 0.018(\hat{n} \cdot \vec{u}). \quad (8)$$

The purpose of the wind correction is to normalize to a zero wind condition. In this case during the northern hemisphere winter, the prevailing wind propagation at Buncefield is eastwards. Therefore, the wind corrected amplitude is less than the observed one. By systematically applying the above method to the HE data set, the following regression relation was obtained

$$P_{\rm wca} = 5.95 \times 10^4 (R_{\rm scaled})^{-1.4072}. \quad (9)$$

In this study, Y is retrieved from the known source–receiver distance, strongest winds at winds at 40 km altitude and observed infrasonic amplitudes. The average peak–peak amplitude of the most dominant stratospheric phase (I_s^3) over DIA is 5.1 Pa. This value is wind corrected to 0.64 Pa with a zonal wind of $+122.7\ {\rm m\,s^{-1}}$ (WE) and meridional wind of $-51.5\ {\rm m\,s^{-1}}$ (NS) from NRL-G2S models at 52.0°N and 2.0°E, approximately halfway between the source and receivers. From the known source–receiver distances the yield estimate is 21.6 (±5) tons TNT equivalent.

5 DISCUSSION

The Buncefield VCE of 2005 December was one of the largest explosions in peace-time Europe. The energy released as seismic waves was widely recorded on seismic instruments in the UK and the Netherlands. Both *P* and *Lg* waves were observed. The absence of Rayleigh waves, which could be expected from a surface explosion source, is possibly explained by high near surface attenuation. The acoustic energy was recorded on seismic stations and infrasound arrays in the Netherlands. Recordings of both seismic and acoustic waves were used to determine the origin time and yield of the explosion, which are both of public interest. The observations further allowed us to interpret the observations and to test models for crustal velocities as well as atmospheric models in a combined seismic and acoustic analysis.

The origin time was determined from seismic *P*-wave arrival times with an estimated formal error of 0.5 s at 90 per cent confidence. Potential sources for the error in origin time are the timing accuracy of the seismic equipment, the accuracy of phase arrival identification and the velocity model. The timing accuracy of the digitising equipment is better than 0.005 s, significantly smaller than the error in picking an arrival at a single station, which is about 0.1 s. The largest residual obtained, when inverting for origin time only is −0.42 s and most of the residuals are larger than the picking error. The residuals are explained by lateral deviation of 'true' crustal wave velocities from the layered velocity models that were used. The residuals are smaller for the Mid Wales model than for other UK models, which means that the Mid Wales model is the most appropriate for this study. However, the use of an alternative velocity model resulted in an origin time difference of only 0.12 s. Inverting for the location of the explosion in addition to the origin time resulted in a minor change of only 0.1 s in origin time (Ottemöller 2006). This demonstrates that the exact location of the explosion within the fuel depot would not make a significant difference to the origin time. The formal uncertainty of 0.5 s can be regarded as a robust maximum. It also demonstrates that the location error for the model and station configuration is only about 1.5 km.

The origin times determined from acoustic arrival times, derived from tropospheric and stratospheric arrivals, respectively, are 8.25 and 4.95 s, before the seismic origin time. The error bounds in the origin time from infrasound modelling are larger than from seismic modelling, because of the larger uncertainties in the atmospheric model. The picking of acoustic phases also has a small contribution to the error, since acoustic onsets are often more emergent than the sharp seismic onsets. However, we have shown that the explosion time can be derived with an accuracy of under 10 s from acoustic arrivals alone.

The energy release estimated from infrasound recordings is equivalent to 21.6 (±5) tons TNT. The determination of yield from the infrasound data was done through comparison with amplitudes observed for a HE data set, after correcting for wind speeds. This comparison is justified as at the observing distance, the differences between HE and VCE are negligible. The main short-coming is the lack of infrasound measurements in other directions from the source.

The infrasound estimate of 21.6 tons can be converted to the equivalent vapour cloud mass. Assuming an explosion efficiency $Y_{\rm eff}$ of 0.1 and combustion heat $\Delta H_{\rm gas}$ of $46.4\ {\rm MJ\,kg^{-1}}$ (e.g. Maremonti *et al.* 1999) and $\Delta H_{\rm TNT}$ of $4.2\ {\rm MJ\,kg^{-1}}$, using

$$W_{\rm gas} = \frac{W_{\rm TNT} \times \Delta H_{\rm TNT}}{\Delta H_{\rm gas} \times Y_{\rm eff}} \quad (10)$$

this is equivalent to an exploded vapour cloud mass of $W_{\rm gas} =$ 19.5 tons, which is 6.5 per cent of the total overflow mass of 300 tons. A VCE only occurs if the gasoline vapour volume is in the range 1.3–6 per cent of the volume. An average ratio of 4 per cent and a gasoline mass of 19.5 tons requires an air volume of about 400 000 m^3. Over an area with 150 m radius, this corresponds to a thickness of about 5.5 m, which is similar to the maximum vapour cloud thickness observed before the explosion. While these estimates do not seem unrealistic, they should be treated with caution due to the large uncertainties.

The yield determined from the infrasound recordings is a measure of the actual VCE. In contrast, from seismic measurements we determined the yield equivalent to a buried chemical explosion that would give the observed seismic amplitudes. This estimate can be useful for engineering purposes. Translation to the actual yield of the VCE would require knowledge of the ground coupling process. The observed magnitude is expected for explosions in the UK for yields of 2–10 tons. The lower limit of 2 tons also results when converting magnitude to energy, and then deriving the yield from energy. The yield range is consistent with conversion relationships obtained elsewhere (Murphy 1981; Evernden *et al.* 1986; Ringdal

et al. 1992). The upper limit of 25 tons derived from ground velocity amplitudes is even higher than the infrasound estimate and probably overestimated.

Our infrasound modelling suggests that all stations may be expected to record acoustic energy from the explosion, assuming the modelled boundaries of the regions of bounce points are not that sharp in reality. This argument is supported by the fact that ray tracing is a high frequency approach, used in this low frequency propagation modelling. Stations showing no acoustic energy either have high noise levels or are less well suited to measure atmospheric waves because of site specific characteristics such as placement with respect to atmospheric exposure. Stations having multiple arrivals to the east of Buncefield have measured additional I_s phases, while I_t phases arrive at stations to the west. No stations with multiple arrivals are present within the shadow zone for I_t and I_s arrivals. The predicted shadow zone for I_t returns appears somewhat (roughly 20 km) larger than follows from the observations. Although boundaries are probably not that sharp, it shows the ability of infrasound to validate or derive atmospheric models.

6 CONCLUSIONS

We have demonstrated that the combined analysis and interpretation of seismic and acoustic observations helps to constrain the uncertainties when estimating the origin time, location and size of explosions. Knowing the location, the Buncefield explosion was used to verify existing models, which helps to understand uncertainties for explosions of unknown location. The main outcome from this work was:

(i) The origin time was 06:01:31.45 (±0.5 s) (UTC) determined from *P*-wave arrival times and a velocity model for Mid Wales. The origin times determined from infrasound phases observed at seismic station in the UK were 5–8 s before the seismic origin time.

(ii) The explosion yield determined from an infrasound recording in the Netherlands was 21.6 (±5) tons TNT.

(iii) The observed seismic amplitudes are comparable to those generated by a buried explosion of 2–10 tons TNT.

(iv) Interpretation of acoustic waves observed at the seismic stations and an infrasound array was possible based on atmospheric ray tracing. The observed acoustic wave types are refracted within the troposphere, stratosphere and thermosphere. The observations of acoustic waves as function of azimuth and distance are explained by the the atmospheric model for the time of the explosion.

ACKNOWLEDGMENTS

This study was partly supported by the Health & Safety Laboratory. Data from station WOL was kindly provided by AWE and Guralp Systems. Data were also available from stations run in the UK by Beal High School and Hailey Hall School. Reviews by Brian Baptie and David Booth helped to improve the manuscript. This paper is published with permission of the Executive Director of the British Geological Survey (NERC). The Royal Netherlands Airforce is thanked for their contribution to DIA. The contribution of NRL-G2S atmospheric models by Doug Drob is greatly appreciated.

REFERENCES

Andrews, D., Holton, J. & Leovy, C., 1987. *Middle Atmosphere Dynamics,* Academic Press Inc., Orlando.

Assumpção, M. & Bamford, D., 1978. LISPB V. Studies of crustal shear waves, *Geophys. J. R. astr. Soc.,* **54,** 61–73.

Bamford, D., Nunn, K., Prodehl, C. & Jacob, B., 1978. LISPB-IV, Crustal structure of Northern Britain, *Geophys. J. R. astr. Soc.,* **54,** 43–60.

Bass, H. & Sutherland, L., 2004. Atmospheric absorption in the atmosphere up to 160 km, *J. acoust. Soc. Am.,* **115,** 1012–1032.

Booth, D., Bott, J. & O'Mongain, A., 2001. The UK seismic velocity model for earthquake location—a baseline review, Internal Report IR/01/188, British Geological Survey, Edinburgh, UK.

Brown, D., Katz, C., Le Bras, R., Flanagan, M., Wang, J. & Gault, A., 2002. Infrasonic signal detection and source location at the prototype data centre, *Pure appl. Geophys.,* **159,** 1081–1125.

Buland, R. & Chapman, C., 1983. The computation of seismic travel times, *Bull. seism. Soc. Am.,* **73,** 1271–1302.

Davidson, M. & Whitaker, R.W., 1992. Miser's Gold, Tech. Rep. LA-12074-MS UC-741, LANL.

Drob, D.P., Picone, J.M. & Garcés, M., 2003. Global morphology of infrasound propagation, *J. geophys. Res.,* **108,** (D21), 4680, doi:10.1029/2002JD003307.

Edwards, J. & Blundell, D., 1984. Summary of seismic refraction experiments in the English Channel, Celtic Sea and St George's Channel, Marine Geophysics Report 144, British Geological Survey, UK.

Evans, J.R., 1999. Blasts from seismic refraction experiments, Technical Report, Commercial in confidence WL/99/09C, British Geological Survey.

Evernden, J., Archambeau, C. & Cranswick, E., 1986. An evaluation of seismic decoupling and underground nuclear test monitoring using high-frequency seismic data, *Rev. Geophys.,* **24,** 143–215.

Evers, L. & Haak, H., 2007. Infrasonic forerunners: exceptionally fast acoustic phases, *Geophys. Res. Lett.,* **34,** L10806.

Evers, L., Ceranna, L., Haak, H., Le Pichon, A. & Whitaker, R., 2007. A seismo-acoustic analysis of the gas-pipeline explosion near Ghislenghien in Belgium, *Bull. seism. Soc. Am.,* **97,** 417–425.

Garcés, M., Hansen, R. & Lindquist, K., 1998. Traveltimes for infrasonic waves propagating in a stratified atmosphere, *Geophys. J. Int.,* **135,** 255–263.

Gossard, E. & Hooke, W., 1975. *Waves in the Atmosphere,* Elsevier Scientific Publishing Company, Amsterdam.

Green, D., Bowers, D., Drob, D. & Hort, M., 2006. The Buncefield oil depot explosion: extending signal coverage using airwaves recorded on seismometers, in *2006 Infrasound Technology Workshop,* University of Alaska Fairbanks, Abstract.

Health and Safety Executive, 1975. The Flixborough Disaster: Report of the Court of Inquiry, Tech. rep., HMSO.

Health and Safety Executive, 1997. The explosion and fires at the Texaco Refinery, Milford Haven, 24 July 1994: a report of the investigation by the Health and Safety Executive into the explosion and fires on the Pembroke Cracking Company Plant at the Texaco Refinery, Milford Haven on 24 July 1994, Tech. rep., Health and Safety Executive.

Hedin, A. *et al.* 1996. Empirical wind model for the upper, middle and lower atmosphere, *J. Atmos. Terr. Phys.,* **58,** 1421–1447.

Herrmann, R.B. & Wang, C.Y., 1985. A comparison of synthetic seismograms, *Bull. seism. Soc. Am.,* **75,** 41–56.

Hutton, L.K. & Boore, D., 1987. The Ml scale in Southern California, *Bull. seism. Soc. Am.,* **77,** 2074–2094.

Ichinose, G.A., Smith, K.D. & Anderson, J.G., 1999. Seismic analysis of the 7 January 1998 chemical plant explosion at Kean Canyon, Nevada, *Bull. seism. Soc. Am.,* **89**(4), 938–945.

Jacob, B. & Neilson, G., 1977. Magnitude determination on Lownet, Global Seismology Internal Report 86, British Geological Survey.

Khalturin, V.I., Rautian, T.G. & Richards, P.G., 1998. The seismic signal strength of chemical explosions, *Bull. seism. Soc. Am.,* **88**(6), 1511–1524.

Koper, K.D., Wallace, T.C. & Aster, R.C., 2003. Seismic recordings of the Carlsbad, New Mexcio, pipeline explosion of 19 August 2000, *Bull. seism. Soc. Am.,* **93**(4), 1427–1432.

Lahr, J., 1999. Table-top earthquakes, Open-file report, U.S. Geological Survey.

Lienert, B.R., 1994. Hypocenter 3.2: a computer program for locating earthquakes locally, regionally and globally, Tech. rep., Hawaii Institute of Geophysics & Planetology, Honolulu.

Lienert, B.R.E. & Havskov, J., 1995. A computer program for locating earthquakes both locally and globally, *Seism. Res. Lett.,* **66,** 26–36.

Maremonti, M., Russo, G., Salzano, E. & Tufano, V., 1999. Post-accident analysis of vapour cloud explosions in fuel storage areas, *Trans IchemE,* **77**(B), 360–365.

Melton, B. & Bailey, L., 1957. Multiple signal correlators, *Geophysics,* **XXII,** 565–588.

Murphy, J., 1981. P-wave coupling of underground explosions in various geologic media, in *Identification of Seismic Sources—Earthquake or Explosion,* pp. 225–245, eds Husebye, E. & Mykkeltveit, S., Reidel, Dordrecht.

Ottemöller, L., 2006. Timing of the explosion at the Buncefield Fuel Depot, 11 December 2005, Commissioned Report CR/06/038, British Geological Survey, Edinburgh, UK.

Powell, T., 2006a. The Buncefield Investigation, progress report, Tech. rep., Buncefield Major Incident Investigation.

Powell, T., 2006b. The Buncefield Investigation, Second progress report, Tech. rep., Buncefield Major Incident Investigation.

Powell, T., 2006c. The Buncefield Investigation, Third progress report, Tech. rep., Buncefield Major Incident Investigation.

Ringdal, F., Marshall, P. & R.W., A., 1992. Seismic yield determination of Soviet underground nuclear explosions at the Shagan River test site, *Geophys. J. Int.,* **109,** 65–77.

Smart, E. & Flinn, E., 1971. Fast frequency-wavenumber analysis and Fisher signal detection in real-time infrasonic array data processing, *Geophys. J. R. astr. Soc.*, **26,** 279–284.

Starovoit, Y.O. & Martysevich, P.N., 2005. Different observed mechanisms of correaltion between seismic and pressure signals, *Inframatics*, **9,** 11–16.

Stein, S. & Wysession, M., 2003. *An Introduction to Seismology, Earthquakes, and Earth Structure,* Blackwell Publishing Ltd, Oxford, UK.

Tang, M.J. & Baker, Q.A., 1999. A new set of blast curves from vapor cloud explosion, *Process Saf. Progr.*, **18**(3), 235–240.

Wang, C.E. & Herrmann, R.B., 1980. A numerical study of P-, SV- and SH-wave generation in a plain layered medium, *Bull. seism. Soc. Am.*, **70,** 1015–1036.